Gradient-based reconstruction of molecular Hamiltonians and density matrices from time-dependent quantum observables

Wucheng Zhang [1], Ilia Tutunnikov [2], Ilya Sh. Averbukh [2], and Roman V. Krems[1,3,*]

[1]*Department of Chemistry, University of British Columbia, Vancouver, B.C., Canada V6T 1Z1*
[2]*AMOS and Department of Chemical and Biological Physics, The Weizmann Institute of Science, Rehovot 7610001, Israel*
[3]*Stewart Blusson Quantum Matter Institute, Vancouver, B.C., Canada V6T 1Z4*

We consider a quantum system with a time-independent Hamiltonian parametrized by a set of unknown parameters α. The system is prepared in a general quantum state by an evolution operator that depends on a set of unknown parameters P. After the preparation, the system evolves in time, and it is characterized by a time-dependent observable $\mathcal{O}(t)$. We show that it is possible to obtain closed-form expressions for the gradients of the distance between $\mathcal{O}(t)$ and a calculated observable with respect to α, P, and all elements of the system density matrix, whether for pure or mixed states. These gradients can be used in projected gradient descent to infer α, P, and the relevant density matrix from dynamical observables. We combine this approach with random phase wave function approximation to obtain closed-form expressions for gradients that can be used to infer population distributions from averaged time-dependent observables in problems with a large number of quantum states participating in dynamics. The approach is illustrated by determining the temperature of molecular gas (initially, in thermal equilibrium at room temperature) from laser-induced time-dependent molecular alignment.

DOI: 10.1103/PhysRevA.105.L060802

I. INTRODUCTION

Imaging molecular wave packets using quantum measurements represents a major challenge, since molecules have complex energy levels structure, requiring large basis sets to describe dynamics. While several approaches, whether equivalent to quantum state tomography [1–3] or least-squares fitting [4–7], have been demonstrated, they either require sophisticated measurements of angle-resolved observables [5–7], probe a restricted range of molecular states participating in dynamics [4], or can only accommodate a single observable [1–3]. A molecular imaging experiment is further complicated by experimental uncertainties in parameters of the fields used for initial state preparation and/or for probing. It is vital to develop approaches for obtaining simultaneously the preparation and probing field parameters, the Hamiltonian parameters, and quantum states that correspond precisely to experimental observables. This problem can, in principle, be addressed with a combination of quantum state and quantum process tomography (QT) aiming to determine the density matrix and the transformations it undergoes. However, extensions of QT approaches to molecular dynamics are challenging. Filter-diagonalization techniques have been applied to extract the spectral function from time-dependent signals [2,8,9]. An alternative approach is based on optimization of feedback loops widely employed in optimal control applications [5,10,11]. Optimal control is generally concerned with the problem of tuning field parameters to achieve results equivalent to those of quantum inverse problems [12–15].

The convergence of feedback loops can be accelerated with machine learning algorithms such as Bayesian optimization, which has been exploited to obtain molecule-molecule interaction potentials in quantum reaction dynamics [16] and dipole polarizability tensors from molecular orientation measurements [17]. However, an extension of these approaches to quantum state reconstruction requires the feedback parameters to describe the entire density matrix. In this case, the number of feedback parameters grows exponentially with the number of molecular states.

In the present work, we demonstrate an efficient and scalable approach to obtain the density matrix and the parameters of Hamiltonian and state-preparation fields from averaged time-dependent observables, such as molecular alignment or a combination of alignment and orientation. The problem is formulated as estimation of a target vector, representing the observable at discretized time instances, by vectors parametrized by density matrix elements. We show that the gradient of the norm of the difference between the target observables and estimators with respect to the density matrix elements and Hamiltonian parameters can be evaluated analytically. Since density matrix evolution preserves normalization and respects selection rules, we use the gradients thus obtained in a projected gradient descent calculation, where each gradient-driven update is projected to the nearest point in the constrained domain. While the formalism introduced in the next section is general, our numerical examples treat the rotational motion of linear molecules (under rigid rotor approximation) excited by nonresonant laser pulses. We demonstrate the approach by reconstructing the field parameters and the density matrix of a molecular gas from noisy alignment and orientation signals. We show that this

*Corresponding author: rkrems@chem.ubc.ca

technique allows reconstructing the density matrix, either before or after the laser excitation. For molecules at thermal equilibrium, we show that this approach can be used to determine the temperature by measuring molecular alignment as a function of time.

The present work assumes that measured time-dependent observables contain sufficient information to reconstruct the entire density matrix. Care must be taken to ensure this. To illustrate this point, we consider molecules excited by two delayed cross-polarized laser pulses. We find that one requires three different observables to reconstruct the resulting density matrix. Extensions of the present approach to include vibrational and electronic degrees of freedom may require more observables. Whether there exist molecular density matrices that cannot, in principle, be uniquely reconstructed from a set of time-dependent observables remains an open question that we leave for future work.

II. THEORY

A. Gradient evaluation

We consider a quantum system with the density operator $\hat{\rho}(t)$ and the time-independent Hamiltonian $\hat{H}(\alpha)$ yielding the propagator $\hat{U}(t)$ so that $\hat{\rho}(t) = \hat{U}(t)\hat{\rho}(t=0)\hat{U}^\dagger(t)$. Here, α is a set of parameters determining the eigenspectrum of $\hat{H}$. Before interaction with an external field, the system is in an unknown mixture of quantum states

$$\hat{\rho}_{\text{ini}} = \sum_j p_j |\chi_j\rangle \langle \chi_j|, \tag{1}$$

where $|\chi_j\rangle$ is either an eigenstate of $\hat{H}$ or a coherent superposition of eigenstates of $\hat{H}$. The interaction with the laser field is assumed to be in the impulsive limit, yielding

$$\begin{aligned}\hat{\rho}(t=0) &= \hat{V}(P)\hat{\rho}_{\text{ini}}\hat{V}^\dagger(P) \\ &= \sum_j p_j |\psi_j\rangle \langle \psi_j| = \sum_j p_j \hat{\rho}_j,\end{aligned} \tag{2}$$

where $\hat{V}(P)$ is the interaction-induced transformation, P is a set of unknown interaction parameters, $|\psi_j\rangle = \hat{V}(P)|\chi_j\rangle$, and $\hat{\rho}_j = |\psi_j\rangle \langle \psi_j|$. The goal is to infer α, p_j, P, and $\hat{\rho}_j$ given an observable or a set of observables. Once p_j, P, and $\hat{\rho}_j$ are inferred, $\hat{\rho}_{\text{ini}}$ is fully determined.

We write

$$\hat{\rho}_j = \sum_n \sum_m c_{n,j} c_{m,j}^* |\phi_n\rangle \langle \phi_m|, \tag{3}$$

where $|\phi_n\rangle$ are the eigenstates of $\hat{H}$, and aim to determine the complex valued coefficients $c_{n,j}$ $\forall n$ and j. For a given j, we arrange the coefficients $c_{n,j}$ in a column vector $\boldsymbol{\psi}_j$ and introduce $\boldsymbol{a} = \text{Re}(\boldsymbol{\psi}_j)$ and $\boldsymbol{b} = \text{Im}(\boldsymbol{\psi}_j)$, which was also used in [18].

The time dependence of an observable is given by

$$\mathcal{O}(t) = \sum_j p_j \text{Tr}[\hat{\rho}_j(t)\hat{O}] = \sum_j p_j \mathcal{O}_j(t). \tag{4}$$

We discretize time t into K values and aim to minimize

$$E = \sum_{c=1}^K |\mathcal{O}(t_c) - \mathcal{O}_{\text{ref}}(t_c)|^2, \tag{5}$$

where $\mathcal{O}(t_c)$ is the observable at time t_c calculated for a trial set of parameters and $\mathcal{O}_{\text{ref}}(t_c)$ is an experimental measurement of $\mathcal{O}$ at $t = t_c$. For the numerical examples in this work, we generate $\mathcal{O}_{\text{ref}}(t_c)$ by rigorous quantum calculations with known parameters. These parameters are then inferred using the proposed method, relying on no other information than the reference signal.

The gradients of E with respect to p_j, $\boldsymbol{a}$, $\boldsymbol{b}$, and P can be written as follows:

$$\frac{\partial E}{\partial p_j} = \sum_{c=1}^K 2[\mathcal{O}(t_c) - \mathcal{O}_{\text{ref}}(t_c)]\mathcal{O}_j(t_c), \tag{6}$$

$$\frac{\partial E}{\partial \boldsymbol{a}} = \sum_{c=1}^K 2[\mathcal{O}(t_c) - \mathcal{O}_{\text{ref}}(t_c)]\sum_j p_j \nabla_{\boldsymbol{a}}\mathcal{O}_j, \tag{7}$$

$$\frac{\partial E}{\partial \boldsymbol{b}} = \sum_{c=1}^K 2[\mathcal{O}(t_c) - \mathcal{O}_{\text{ref}}(t_c)]\sum_j p_j \nabla_{\boldsymbol{b}}\mathcal{O}_j, \tag{8}$$

and

$$\frac{\partial E}{\partial P} = \frac{\partial E}{\partial \boldsymbol{a}}\text{Re}\left(\frac{\partial \boldsymbol{\psi}_j}{\partial P}\right) + \frac{\partial E}{\partial \boldsymbol{b}}\text{Im}\left(\frac{\partial \boldsymbol{\psi}_j}{\partial P}\right), \tag{9}$$

where, for simplicity, we assume that P is a single parameter characterizing the strength of the excitation. Generalization to the case when P is a set containing more than one parameter is straightforward. To evaluate $\partial \mathcal{O}_j(t_c)/\partial \boldsymbol{a}$ and $\partial \mathcal{O}_j(t_c)/\partial \boldsymbol{b}$, we apply the results of the Appendix to $\mathcal{O}_j = \langle \psi_j|\hat{U}^\dagger\hat{O}\hat{U}|\psi_j\rangle$ and arrive at

$$\nabla_{\boldsymbol{a}}\mathcal{O}_j = \boldsymbol{U}^\dagger\boldsymbol{\mathcal{O}}\boldsymbol{U}\boldsymbol{\psi}_j + (\boldsymbol{U}^\dagger\boldsymbol{\mathcal{O}}\boldsymbol{U})^T\boldsymbol{\psi}_j^*, \tag{10}$$

$$\nabla_{\boldsymbol{b}}\mathcal{O}_j = i(\boldsymbol{U}^\dagger\boldsymbol{\mathcal{O}}\boldsymbol{U})^T\boldsymbol{\psi}_j^* - i\boldsymbol{U}^\dagger\boldsymbol{\mathcal{O}}\boldsymbol{U}\boldsymbol{\psi}_j, \tag{11}$$

where all operators are represented by matrices in the basis $|\phi_n\rangle$. A related approach, using functional derivatives, was used in inversion problems involving molecular spectroscopic data (e.g., see [19,20]).

We thus obtain analytic gradients with respect to the probabilities of the mixed states p_j, the parameters of the state preparation fields P, and the real and imaginary parts of the expansion coefficients $c_{n,j}$. To obtain physical solutions, these gradients are used in constrained optimization. During the optimization, each gradient-informed update is projected to the nearest point in the subdomain that respects (i) the normalization of p_j and $c_{n,j}$; (ii) selection rules; and (iii) conservation of corresponding quantum numbers.

B. Projected gradient descent

The gradients derived in the previous section can be used in gradient descent optimization. However, because the variables of the optimization are physical parameters, it is necessary to constrain the optimization to ensure that the parameters satisfy physical conditions. For example, the coefficients $c_{n,j}$ or the probabilities p_j must always remain properly

normalized. This can be achieved by means of the projected gradient descent method.

We consider a parameter space $\mathbb{R}^n$ with parameters constrained in the domain $S \subset \mathbb{R}^n$. For example, in the case of probabilities, S is the hyperplane $\sum_j p_j = 1$. The projected gradient descent method enables the optimization of $f(\boldsymbol{x})$ under the constraint $\boldsymbol{x} \in S$ [21]. The algorithm can be summarized as follows:.

(1) Start randomly at $\boldsymbol{x}_0$.

(2) For $k \in \mathbb{Z} \cap [0, \infty)$ and until convergence is reached:

    2.1 Evaluate the gradient $\nabla f(\boldsymbol{x}_k)$.

    2.2 Update $\tilde{\boldsymbol{x}}_{k+1} = \boldsymbol{x}_k - \alpha_k \nabla f(\boldsymbol{x}_k)$ with step size α_k.

    2.3 Project $\tilde{\boldsymbol{x}}_{k+1}$ to the constrained domain by finding $\boldsymbol{x}_{k+1} = \mathrm{argmin}_{\boldsymbol{x} \in S} |\boldsymbol{x} - \tilde{\boldsymbol{x}}_{k+1}|$.

C. Random phase wave function

To construct the full quantum state at time t, the time propagators should be applied to each of the Hamiltonian eigenstates participating in dynamics. However, at high temperature, the number of populated energy states becomes very large, making this approach computationally expensive. For such problems, we combine the gradients derived above with the random phase wave function (RPWF) approach [22–24]. For a system with a large number of $|\chi_n\rangle$ and associated population probabilities, one can introduce a RPWF:

$$|\alpha_k\rangle = \sum_n e^{-i\alpha_k^n} |\chi_n\rangle \sqrt{p_n}, \qquad (12)$$

where the phase α_k^n is randomly sampled from an interval $[0, 2\pi]$. The state preparation field is then assumed to apply to $|\alpha_k\rangle$ to produce the density operator $\hat{\rho}_k$ and the observable $\mathcal{O}_k(t) = \mathrm{Tr}[\hat{\rho}_k(t)\hat{O}]$. The average

$$\langle\hat{O}\rangle_{\mathrm{RPWF}}(t) = \frac{1}{N}\sum_{k=1}^{N}\mathcal{O}_k(t) \qquad (13)$$

is known to converge to the exact result in the limit of large N [24]. By linearity,

$$\langle\hat{O}\rangle_{\mathrm{RPWF}}(t) = \langle p|\hat{M}|p\rangle, \qquad (14)$$

where $\boldsymbol{M} = N^{-1}\sum_{k=1}^{N}\boldsymbol{\Theta}_k^\dagger\boldsymbol{\Pi}^\dagger\boldsymbol{V}^\dagger\boldsymbol{U}^\dagger(t)\boldsymbol{O}\boldsymbol{U}(t)\boldsymbol{V}\boldsymbol{\Pi}\boldsymbol{\Theta}_k$, with $\boldsymbol{\Theta}_k$ being a diagonal matrix of $\exp(-i\alpha_k^n)$, the elements of $\boldsymbol{\Pi}$ given by $\langle\phi_m|\chi_n\rangle$, and $|p\rangle = \sum_j \sqrt{p_j}|\chi_j\rangle$. Thus the gradient can be evaluated as

$$\frac{\partial E}{\partial \boldsymbol{p}} = \sum_{c=1}^{K} 2[\langle\hat{O}\rangle_{\mathrm{RPWF}}(t_c) - \mathcal{O}_{\mathrm{ref}}(t_c)](\boldsymbol{M} + \boldsymbol{M}^\top)\boldsymbol{p}, \qquad (15)$$

where $\boldsymbol{p}$ is a column vector of $\sqrt{p_j}$.

III. RESULTS

We now illustrate the proposed approach by considering several problems of increasing complexity. We consider an ensemble of homonuclear rigid diatomic molecules with $\hat{H} = \hat{J}^2/(2I)$, where $\hat{J}$ is the angular momentum operator, and I is the moment of inertia. The spectrum (in atomic units) and eigenstates of $\hat{H}$ are $J(J+1)/(2I)$ and $|J,M\rangle$, where M is the eigenvalue of $\hat{J}_Z$, the Z component of $\hat{J}$ [25,26]. We use
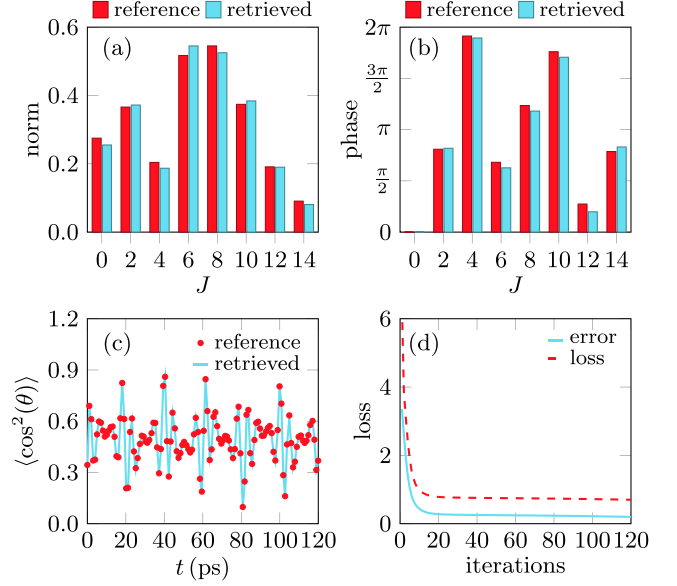

FIG. 1. Comparison of reference [red (dark gray)] and reconstructed [blue (light gray)] values of the norm (a) and phase (b) of C_J. The reconstruction is based on the $\langle\cos^2(\theta)\rangle(t)$ signal, including 3% Gaussian noise, as shown in (c). Panel (d) illustrates the convergence of the target vector estimation error and the loss function, i.e., error with $L2$ regularization.

spherical harmonics $Y_{JM}(\theta, \varphi)$ with θ and φ defined as in Ref. [25] to represent $|J, M\rangle$.

A. Pure state: Excitation by a single linearly polarized laser pulse

First, we consider molecules at zero initial temperature in $|J, M\rangle = |0, 0\rangle$ excited by a nonresonant femtosecond pulse linearly polarized along the Z axis. The pulse creates coherent superpositions of a large number of $|J, M = 0\rangle$ states and induces molecular alignment [26–29]. In the impulsive approximation, $V(P) = \exp[iP\cos^2(\theta)]$, where P is the interaction strength parameter [30]. The matrix representation of $V(P)$ in the basis $|JM\rangle$ can be evaluated using the expansion of $\exp[iP\cos^2(\theta)]$ in spherical harmonics [31] and applying the Wigner-Eckart theorem [25]. We set $P = 8.278$.

We compute a reference time-dependent degree of alignment quantified by $\langle\cos^2(\theta)\rangle(t)$ and modulate it by adding 3% Gaussian noise to simulate an experimental signal $\mathcal{O}_{\mathrm{ref}}(t)$. This reference signal is then used to reconstruct the real and imaginary parts of the probability amplitudes C_J for each $|J, M = 0\rangle$ state in the wave packet. To account for noise, we regularize the objective function in Eq. (5) by adding the $L2$ norm $|\boldsymbol{\psi}|$, as is commonly done in ridge regression in machine learning [32]. For this problem, we only require the gradients given by Eqs. (10) and (11). Figure 1 illustrates that projected gradient descent steered by these derivatives reconstructs both the norm and the phase of each wave packet component with as few as ten iterations.

FIG. 3. Convergence of the inferred temperature and the target vector estimation error (inset) for the $\langle \cos^2(\theta) \rangle (t)$ signal used for Fig. 2.
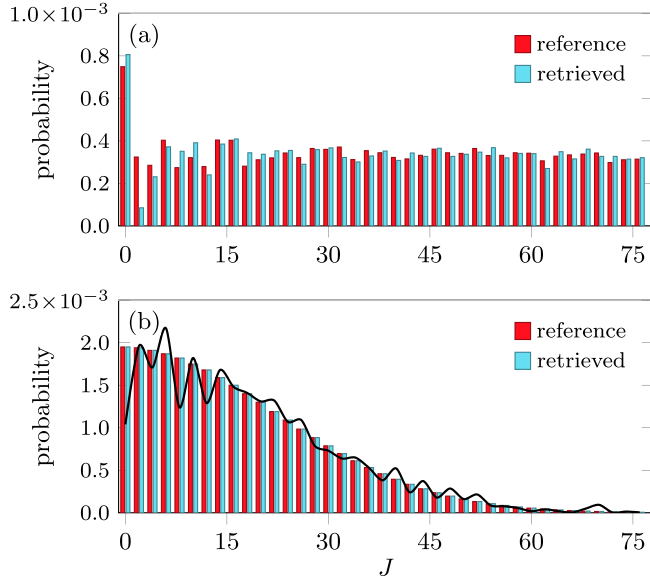

FIG. 2. Comparison of reference [red (dark gray)] and reconstructed [blue (light gray)] probabilities for (a) a mixture consisting of 3003 rotational states, $|JM\rangle$ with even $J \leqslant 76$ with random populations drawn from a uniform distribution; and (b) a thermal ensemble of molecules with $T = 300$ K. The reconstruction is based on $\langle \cos^2(\theta) \rangle (t)$ simulated using the RPWF approach. The solid curve in (b) is obtained without temperature gradients or any information on the relative population probabilities.

B. Thermal ensembles

We now consider ensembles of molecules initially in mixed states including a large number of molecular rotational states. We consider two cases: (i) an ensemble of 3003 states $|J, M\rangle$ with even $J \leqslant 76$, where the initial populations are randomly drawn from a uniform distribution; and (ii) a thermal ensemble of molecules at room temperature. The reference signals for these ensembles are computed using the exact time propagation of each molecular state (up to $J = 76$) participating in dynamics. The inferred probabilities are obtained using Eq. (15) based on RPWF with $N = 30$, which leads to convergent results and is sufficient to recover the probability distribution. Figure 2 illustrates the efficiency of our approach applied to two different initial population distributions. We further illustrate the generality of our approach by the solid line in Fig. 2(b) showing the results for a thermal ensemble obtained without any information about relative population probabilities.

For a thermal ensemble, the population probability gradients [see Eq. (15)] can be extended by the chain rule to obtain the temperature gradient

$$\frac{dE}{dT} = \frac{dE}{d\boldsymbol{p}} \frac{d\boldsymbol{p}}{dT}, \tag{16}$$

yielding a formalism for determining the temperature directly from an observed laser-induced alignment signal. The bars in Fig. 2(b) illustrate the probabilities inferred for initial Boltzmann distribution. The difference between the solid curve and the bars shows the improvement of the inference resulting from the inclusion of the temperature gradients. The conver-
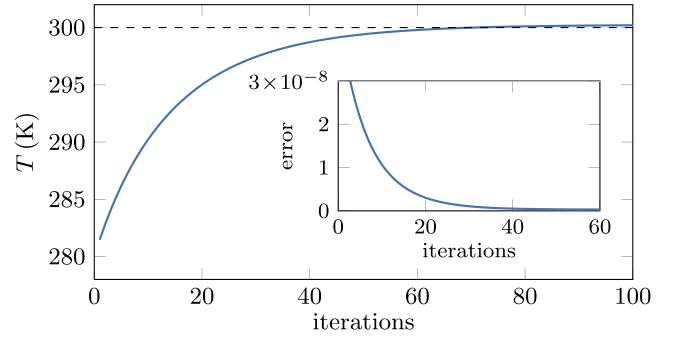
gence of inferred temperature for the thermal ensemble in Fig. 2(b) is illustrated in Fig. 3. The slower convergence of T compared to the error is due to the exponential relation $p_j \sim \exp[-E/(k_B T)]$ (k_B is the Boltzmann constant) where the small change in error corresponds to the large change in T near the minimum. A related problem of inferring rotational temperature from an alignment signal was recently considered experimentally in Ref. [33]. The rotational temperature of molecules after impulsive excitation was obtained by least-squares fitting, restricting the application to cold gases (< 58 K), with accuracy of ≈ 2–4 K, likely limited by experimental noise. The present approach applies to a wider range of T and allows for control of inference accuracy through the proper choice of $L2$ regularization, the number of iterations, and N.

C. Pure state excited by two cross-polarized laser pulses

We now consider a molecular ensemble excited by two delayed cross-polarized laser pulses: the first polarized along the X axis and the second in the XY plane at $45°$ to the X axis. Such an excitation induces molecular unidirectional rotation [30,34,35], i.e., creates a wave packet with coherences between states with different J and M. This significantly enlarges the corresponding density matrices and makes the inverse problem nonunique: a single alignment signal, $\langle \cos^2(\theta) \rangle$, is not sufficient to determine the probability amplitudes C_{JM} for all $|JM\rangle$. The nonuniqueness is resolved by including multiple reference signals into the objective function in Eq. (5). We find that all C_{JM} can be reconstructed if the reference signal includes simultaneously three observables: $\langle \cos^2(\theta) \rangle$, $\langle \cos^2(\phi) \rangle$, and $\langle \sin^2(\theta) \sin(2\phi) \rangle$. All of these observables can be probed either optically or using Coulomb explosion-based methods [6,27,29,36–38]. Recently developed experimental techniques, such as the cold target recoil ion momentum spectroscopy (COLTRIMS) [34,39,40], allow one to probe these observables simultaneously. Figure 4 illustrates the norm and phase of each of the coefficients C_{JM} inferred from a combination of these observables. The molecular state number refers to $|JM\rangle$ states ordered as $|0, 0\rangle$, $|1, -1\rangle$, $|1, 0\rangle$, $|1, 1\rangle$, ...
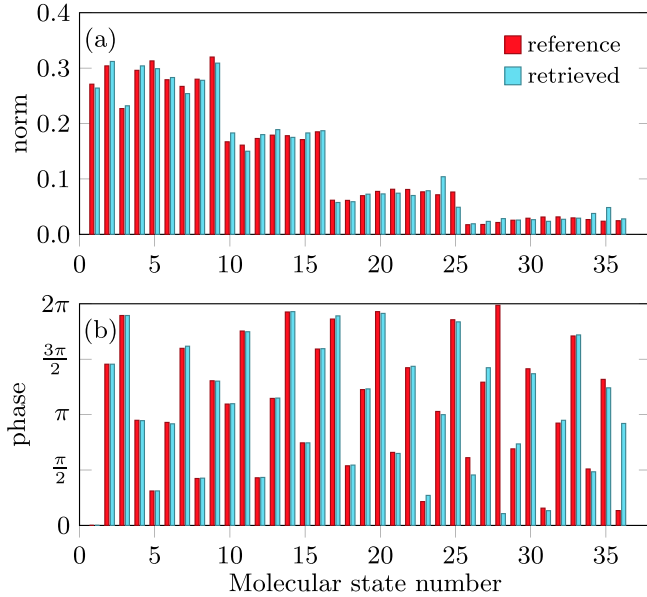
FIG. 4. Comparison of reference [red (dark gray)] and reconstructed [blue (light gray)] values of the norm (a) and phase (b) of C_{JM} for the rotational wave packet produced by excitation of molecules initially in $|J, M\rangle = |0, 0\rangle$ with two cross-polarized pulses. The molecular states are arranged in order of increasing J and, for a given J, in order of increasing M. The wave-packet reconstruction is based on a combination of three signals: $\langle \cos^2(\theta) \rangle$, $\langle \cos^2(\phi) \rangle$, and $\langle \sin^2(\theta) \sin(2\phi) \rangle$ used simultaneously. Notice that the phase difference for molecular state 28 appears to be large as a consequence of constraining the phase to the interval $[0, 2\pi)$.

D. Simultaneous reconstruction

Finally, we consider a problem of simultaneous reconstruction of the Hamiltonian parameters (α and P) and the populations of a mixed state from a time-dependent alignment signal following a single-pulse excitation. We treat the molecular moment of inertia I and the excitation strength parameter P of the linearly polarized (along the Z axis) preparation laser pulse as unknown variables and supplement the gradients to include the derivatives with respect to P and I. We write the derivatives in Eq. (9) as

$$\frac{\partial \boldsymbol{\psi}_j}{\partial P} = \frac{\partial \boldsymbol{V}(P)}{\partial P} \boldsymbol{\chi}_j, \tag{17}$$

where $\boldsymbol{\chi}_j$ is a vector of $\langle \phi_n | \chi_j \rangle$. In addition, we express

$$\frac{\partial \mathcal{O}_j}{\partial I} = \frac{\partial \mathcal{O}_j}{\partial \boldsymbol{h}} \frac{\partial \boldsymbol{h}}{\partial I}, \tag{18}$$

where $\boldsymbol{h}$ is a vector of eigenenergies, $h_J = J(J+1)/(2I)$. The first term can be explicitly written as

$$\frac{\partial \mathcal{O}_j}{\partial \boldsymbol{h}} = (it)\boldsymbol{u}^{*\top} \boldsymbol{A}_j \boldsymbol{u} - (it)\boldsymbol{u}^\top \boldsymbol{A}_j^\top \boldsymbol{u}^*, \tag{19}$$

where $\boldsymbol{u}$ is a vector of $\exp(ih_J t)$, $\boldsymbol{A}_j = \boldsymbol{S}_j^\dagger \mathcal{O} \boldsymbol{S}_j$, and $\boldsymbol{S}_j$ is a diagonal matrix of $\langle \phi_n | \psi_j \rangle$. The second term is given by $\partial h_J / \partial I = -J(J+1)/(2I^2)$. We apply Eqs. (9)–(11) and (17)–(19) to evaluate the gradient with respect to P, I, p_j, which are used in projected gradient descent. We consider an alignment signal $\langle \cos^2(\theta) \rangle (t)$ produced by exciting molecules
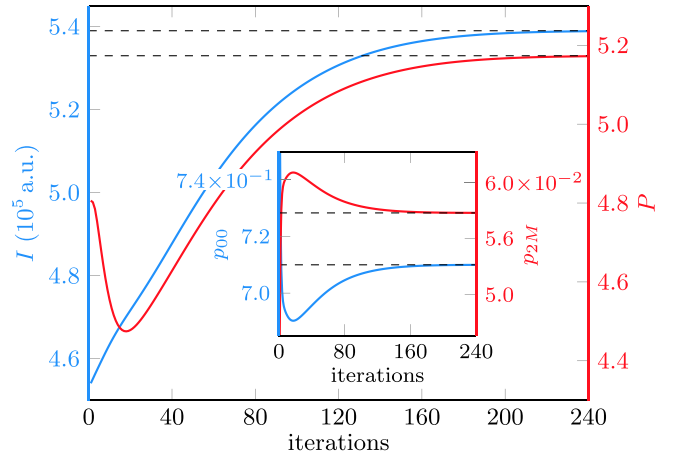

FIG. 5. Convergence of the inferred field parameter P and molecular moment of inertia I, using $\langle \cos^2(\theta) \rangle (t)$. The inset shows the convergence of the probabilities of $|J = 0, M_J = 0\rangle$, $|2, -2\rangle$, $|2, -1\rangle$, $|2, 0\rangle$, $|2, 1\rangle$, and $|2, 2\rangle$ in the initial mixed state. The dashed lines show the reference values to be inferred.

with $I = 539\,010$ a.u. in a mixture of $J = 0$ and $J = 2$ states by linearly polarized pulse with $P = 5.174$ yielding wave packets including rotational states with $J \leqslant 10$. Figure 5 illustrates the convergence of I, P, and the probabilities in the initial mixed state to the corresponding inferred values. Notice that all $|2, M\rangle$ states are equally populated initially.

IV. CONCLUSION

In summary, we have shown that for a time-independent Hamiltonian $\hat{H}$ with spectrum parametrized by α and quantum states prepared by $\hat{V}(P)$ over finite time, it is possible to obtain closed-form expressions for the gradients of the distance between calculated and observed time-dependent signals with respect to α, P, and the elements of the system density matrix. These gradients can be used in projected gradient descent to infer α, P, and the density matrix from dynamical observables, such as molecular alignment or orientation. We have shown that this approach can be combined with random phase wave function approximation, yielding closed-form expressions for gradients that can be used to infer population distributions spanning a large number of molecular states from averaged time-dependent observables. We have illustrated that the temperature of a molecular gas at ambient conditions can be determined optically by probing time dependence of alignment. This demonstrates a way of probing molecular distributions in applications requiring remote sensing and opens up possibilities for solving inverse quantum problems with averaged dynamical observables.

We note that several important questions remain unanswered by this study. While our calculations demonstrate that some density matrices can be reconstructed with several simultaneously measured observables, we believe that the minimum number of observables required for the reconstruction of the full density matrix is generally not known. References [41,42] provided a formula for the minimum number of observables based on the degeneracy of the time evolution operator. In particular, it was suggested that a non-

degenerate system requires d observables, where d is the dimension of the Hilbert space. However, this clearly contradicts our results in Sec. III A and the results in Refs. [4–7]. Further examination is required to investigate what determines the minimum amount of observable information, both in terms of the number of observables and the duration of the time-dependent signals, for the reconstruction of molecular density matrices, including the relationship between the number of observables, symmetries, and parameters of the state-preparation fields. This question is particularly relevant for extensions of the present approach to include vibrational and electronic degrees of freedom.

APPENDIX: DERIVATIVE OF COMPLEX QUADRATIC FORM

Consider $f(\boldsymbol{x}) = \boldsymbol{x}^\dagger \boldsymbol{U} \boldsymbol{x}$, where $\boldsymbol{x}$ is a complex valued column vector and $\boldsymbol{U}$ is a Hermitian matrix:

$$f(\boldsymbol{x}) = \sum_{i,j=1}^{n} x_i u_{ij} x_j = \sum_{i=1}^{n}\left[u_{ii} x_i^2 + \sum_{j \neq i} x_i u_{ij} x_j \right], \quad \text{(A1)}$$

where x_i are the elements of x and u_{ij} are the elements of U. By writing $x_i = a_i + ib_i$, we recast Eq. (A1) as

$$f(\boldsymbol{x}) = \sum_{i=1}^{n}\left[u_{ii}\left(a_i^2 + b_i^2\right) \right.$$
$$\left. + \sum_{j \neq i} u_{ij}(a_i a_j + b_i b_j + i a_i b_j - i b_i a_j) \right]. \quad \text{(A2)}$$

A partial derivative with respect to a_k is

$$\frac{\partial f}{\partial a_k} = 2 u_{kk} a_k + \sum_{j \neq k} u_{kj}(a_j + ib_j) + \sum_{i \neq k} u_{ik}(a_i - ib_i)$$
$$= u_{kk}(a_k + ib_k) + u_{kk}(a_k - ib_k)$$
$$+ \sum_{j \neq k} u_{kj}(a_j + ib_j) + \sum_{i \neq k} u_{ik}(a_i - ib_i)$$
$$= \sum_{j=1}^{n} u_{kj}(a_j + ib_j) + \sum_{i=1}^{n} u_{ik}(a_i - ib_i), \quad \text{(A3)}$$

which yields

$$\nabla_a f(\boldsymbol{x}) = \left[\frac{\partial f}{\partial a_k}\right] = \boldsymbol{U}\boldsymbol{x} + \boldsymbol{U}^\top \boldsymbol{x}^*. \quad \text{(A4)}$$

Similarly,

$$\frac{\partial f}{\partial b_k} = -i\sum_{j=1}^{n} u_{kj}(a_j + ib_j) + i\sum_{i=1}^{n} u_{ik}(a_i - ib_j), \quad \text{(A5)}$$

yielding

$$\nabla_b f(\boldsymbol{x}) = \left[\frac{\partial f}{\partial b_k}\right] = i\boldsymbol{U}^\top \boldsymbol{x}^* - i\boldsymbol{U}\boldsymbol{x}. \quad \text{(A6)}$$

[1] A. S. Mouritzen and K. Mølmer, Quantum state tomography of molecular rotation, J. Chem. Phys. **124**, 244311 (2006).

[2] V. A. Mandelshtam and H. S. Taylor, Harmonic inversion of time signals and its applications, J. Chem. Phys. **107**, 6756 (1997).

[3] D. Avisar and D. J. Tannor, Complete Reconstruction of the Wave Function of a Reacting Molecule by Four-Wave Mixing Spectroscopy, Phys. Rev. Lett. **106**, 170405 (2011).

[4] H. Hasegawa and Y. Ohshima, Quantum State Reconstruction of a Rotational Wave Packet Created by a Nonresonant Intense Femtosecond Laser Field, Phys. Rev. Lett. **101**, 053002 (2008).

[5] X. He, S. Schmohl, and H.-D. Wiemhöfer, Direct observation and suppression effect of lithium dendrite growth for polyphosphazene based polymer electrolytes in lithium metal cells, Chem Electro Chem **6**, 1166 (2019).

[6] E. T. Karamatskos, S. Raabe, T. Mullins, A. Trabattoni, P. Stammer, G. Goldsztejn, R. R. Johansen, K. Długołecki, H. Stapelfeldt, M. J. J. Vrakking, S. Trippel, A. Rouzée, and J. Küpper, Molecular movie of ultrafast coherent rotational dynamics of OCS, Nat. Commun. **10**, 3364 (2019).

[7] K. Ueno, K. Mizuse, and Y. Ohshima, Quantum-state reconstruction of unidirectional molecular rotations, Phys. Rev. A **103**, 053104 (2021).

[8] V. A. Mandelshtam and H. S. Taylor, A low-storage filter diagonalization method for quantum eigenenergy calculation or for spectral analysis of time signals, J. Chem. Phys. **106**, 5085 (1997).

[9] V. A. Mandelshtam and H. S. Taylor, Spectral Analysis of Time Correlation Function for a Dissipative Dynamical System Using Filter Diagonalization: Application to Calculation of Unimolecular Decay Rates, Phys. Rev. Lett. **78**, 3274 (1997).

[10] R. S. Judson and H. Rabitz, Teaching Lasers to Control Molecules, Phys. Rev. Lett. **68**, 1500 (1992).

[11] A. P. Peirce, M. A. Dahleh, and H. Rabitz, Optimal control of quantum-mechanical systems: Existence, numerical approximation, and applications, Phys. Rev. A **37**, 4950 (1988).

[12] Boris N. Zakhariev and V. M. Chabanov, New situation in quantum mechanics (wonderful potentials from the inverse problem), Inverse Probl. **13**, R47 (1997).

[13] R. J. Leroy and R. B. Bernstein, Dissociation energies of diatomic moleculles from vibrational spacings of higher levels: application to the halogens, Chem. Phys. Lett. **5**, 42 (1970).

[14] A. Pashov, W. Jastrzebski, and P. Kowalczyk, Construction of potential curves for diatomic molecular states by the IPA method, Comput. Phys. Commun. **128**, 622 (2000).

[15] S. M. Kirschner and J. K. Watson, RKR potentials and semi-classical centrifugal constants of diatomic molecules, J. Mol. Spectrosc. **47**, 234 (1973).

[16] R. A. Vargas-Hernández, Y. Guan, D. H. Zhang, and R. V. Krems, Bayesian optimization for the inverse scattering problem in quantum reaction dynamics, New J. Phys. **21**, 022001 (2019).

[17] Z. Deng, I. Tutunnikov, I. Sh. Averbukh, M. Thachuk, and R. V. Krems, Bayesian optimization for inverse problems in time-dependent quantum dynamics, J. Chem. Phys. **153**, 164111 (2020).

[18] J. P. Palao and R. Kosloff, Optimal control theory for unitary transformations, Phys. Rev. A **68**, 062308 (2003).

[19] R. Baer and R. Kosloff, Obtaining the excited-state potential by inversion of photodissociation absorption spectra, Chem. Phys. Lett. **200**, 183 (1992).

[20] H. Heo, T. Ho, K. K. Lehmann, and H. Rabitz, Regularized inversion of diatomic vibration-rotation spectral data: A functional sensitivity analysis approach, J. Chem. Phys. **97**, 852 (1992).

[21] A. Beck, *Introduction to Nonlinear Optimization: Theory, Algorithms, and Applications with MATLAB* (SIAM, Philadelphia, PA, 2014).

[22] D. Gelman and R. Kosloff, Simulating dissipative phenomena with a random phase thermal wavefunctions, high temperature application of the surrogate Hamiltonian approach, Chem. Phys. Lett. **381**, 129 (2003).

[23] M. Nest and R. Kosloff, Quantum dynamical treatment of inelastic scattering of atoms at a surface at finite temperature: The random phase thermal wave function approach, J. Chem. Phys. **127**, 134711 (2007).

[24] S. Kallush and S. Fleischer, Orientation dynamics of asymmetric rotors using random phase wave functions, Phys. Rev. A **91**, 063420 (2015).

[25] R. Zare, *Angular Momentum: Understanding Spatial Aspects in Chemistry and Physics* (Wiley, New York, 1988).

[26] R. V. Krems, *Molecules in Electromagnetic Fields: From Ultracold Physics to Controlled Chemistry* (Wiley, New York, 2018).

[27] H. Stapelfeldt and T. Seideman, *Colloquium*: Aligning molecules with strong laser pulses, Rev. Mod. Phys. **75**, 543 (2003).

[28] S. Fleischer, Y. Khodorkovsky, E. Gershnabel, Y. Prior, and I. Sh. Averbukh, Molecular alignment induced by ultrashort laser pulses and its impact on molecular motion, Isr. J. Chem. **52**, 414 (2012).

[29] C. P. Koch, M. Lemeshko, and D. Sugny, Quantum control of molecular rotation, Rev. Mod. Phys. **91**, 035005 (2019).

[30] S. Fleischer, Y. Khodorkovsky, Y. Prior, and I. Sh. Averbukh, Controlling the sense of molecular rotation, New J. Phys. **11**, 105039 (2009).

[31] M. Leibscher, I. Sh. Averbukh, and H. Rabitz, Enhanced molecular alignment by short laser pulses, Phys. Rev. A **69**, 013402 (2004).

[32] J. F. Trevor Hastie and Robert Tibshirani, *The Elements of Statistical Learning: Data Mining, Inference, and Prediction* (Springer, New York, 2009).

[33] M. Oppermann, S. J. Weber, and J. P. Marangos, Characterising and optimising impulsive molecular alignment in mixed gas samples, Phys. Chem. Chem. Phys. **14**, 9785 (2012).

[34] K. Lin, Q. Song, X. Gong, Q. Ji, H. Pan, J. Ding, H. Zeng, and J. Wu, Visualizing molecular unidirectional rotation, Phys. Rev. A **92**, 013410 (2015).

[35] K. Mizuse, K. Kitano, H. Hasegawa, and Y. Ohshima, Quantum unidirectional rotation directly imaged with molecules, Sci. Adv. **1**, e1400185 (2015).

[36] V. Renard, M. Renard, S. Guérin, Y. T. Pashayan, B. Lavorel, O. Faucher, and H. R. Jauslin, Postpulse Molecular Alignment Measured by a Weak Field Polarization Technique, Phys. Rev. Lett. **90**, 153601 (2003).

[37] O. Faucher, B. Lavorel, E. Hertz, and F. Chaussard, Optically probed laser-induced field-free molecular alignment, in *Progress in Ultrafast Intense Laser Science VII*, edited by K. Yamanouchi, D. Charalambidis, and D. Normand (Springer, Berlin, Heidelberg, 2011), pp. 79–108.

[38] R. Damari, S. Kallush, and S. Fleischer, Rotational Control of Asymmetric Molecules: Dipole- Versus Polarizability-Driven Rotational Dynamics, Phys. Rev. Lett. **117**, 103001 (2016).

[39] R. Dörner, V. Mergel, O. Jagutzki, L. Spielberger, J. Ullrich, R. Moshammer, and H. Schmidt-Böcking, Cold Target Recoil Ion Momentum Spectroscopy: A "momentum microscope" to view atomic collision dynamics, Phys. Rep. **330**, 95 (2000).

[40] L. Xu, I. Tutunnikov, L. Zhou, K. Lin, J. Qiang, P. Lu, Y. Prior, I. Sh. Averbukh, and J. Wu, Echoes in unidirectionally rotating molecules, Phys. Rev. A **102**, 043116 (2020).

[41] A. Jamiołkowski, Minimal number of operators for observability of *N*-level quantum systems, Int. J. Theor. Phys. **22**, 369 (1983).

[42] A. Jamiołkowski, On a stroboscopic approach to quantum tomography of qudits governed by Gaussian semigroups, Open Syst. Inf. Dyn. **11**, 63 (2004).